

Continuous signal sparse encoding using analog neuromorphic variability

Filippo Costa^{1,2}, Chiara De Luca^{1,3}

¹ Institute of Neuroinformatics, University of Zurich and ETH Zurich, Winterthurerstrasse 190 CH-8057 Zurich, Switzerland

² Department of Neurosurgery, University Hospital Zurich, Rämistrasse 100 Zurich, Switzerland

³ Digital Society Initiative, University of Zurich, Rämistrasse 69 CH-8001 Zurich, Switzerland

E-mail: filippo.costa@usz.ch, chiara.deluca@ini.uzh.ch

Abstract. Achieving fast and reliable temporal signal encoding is crucial for low-power, always-on systems. While current spike-based encoding algorithms rely on complex networks or precise timing references, simple and robust encoding models can be obtained by leveraging the intrinsic properties of analog hardware substrates.

We propose an encoding framework inspired by biological principles that leverages intrinsic neuronal variability to robustly encode continuous stimuli into spatio-temporal patterns, using at most one spike per neuron.

The encoder has low model complexity, relying on a shallow network of heterogeneous neurons. It relies on an internal time reference, allowing for continuous processing. Moreover, stimulus parameters can be linearly decoded from the spiking patterns, granting fast information retrieval. Our approach, validated on both analog neuromorphic hardware and simulation, demonstrates high robustness to noise, spike jitter, and reduced heterogeneity. Consistently with biological observations, we observed the spontaneous emergence of patterns with stereotyped spiking order. The proposed encoding scheme facilitates fast, robust and continuous information processing, making it well-suited for low-power, low-latency processing of temporal data on analog neuromorphic substrates.

Keywords: spiking encoder, heterogeneity, neuromorphic

Introduction

Neuronal communication is inherently spike-based, with neurons transmitting information through sequences of action potentials (spikes) that encode sensory inputs as discrete temporal events. This spike-timing mechanism underpins the dynamic and precise nature of neural processing, enabling efficient encoding and representation of stimuli across diverse contexts [1, 2]. Also, neuronal responses exhibit a high degree of variability, where even neurons within the same functional column can exhibit highly variable spiking behaviors in response to identical stimuli [3, 4].

Heterogeneity in neural responses is not merely a byproduct of noisy processes but a critical feature of biological systems. It has been demonstrated [3] that the high variability in intrinsic response properties of individual cells changes the structure of neuronal correlations, enhancing the information encoded in population activity and improving sensory coding [5]. Stereotyped spiking patterns, observed in the cortex, provide a scaffold for information processing and transmission [6, 7, 8]. These patterns represent coordinated firing across the network and can be thought of as core neural events that likely encode important information, carrying critical information about the timing and nature of sensory inputs [9, 8]. These events are thought to play a key role in compact and efficient information encoding. These dynamics highlight the potential of variability-driven mechanisms to support compact, efficient, and robust information encoding.

From a computational perspective, leveraging neuronal variability and spike-based processing for encoding algorithms has significant implications for improving the efficiency and

robustness of signal processing. Learning with variability has been shown to lead to more stable and robust results in simulated spiking neural networks across various tasks, especially those with rich temporal structures [10, 11], also allowing for the emergence of computationally specialized networks [12, 4]. This heterogeneity also applies to the spiking encoding of sensory signals, typically continuous and temporally varying [3, 13].

Multiple studies have explored optimal ways to exploit this spike-based processing in noisy environments to encode analog signals [14] and map amplitude information into time sequences [15, 16, 17, 18]. Existing spike-based encoding methods demonstrated energy-efficient and low-latency information coding through precise spike timing [17], providing a flexible framework to understand how neurons can effectively process temporal information in a changing environment [19, 20]. Fast spike-based processing can be obtained with time-to-first-spike (TTFS) coding algorithms that use at most one spike per neuron but require an external time reference [21, 22]. Reliable computation can also be obtained with recurrently-connected networks with balanced excitatory-inhibitory neurons [23, 24] and spatio-temporal spiking patterns [25].

Building on these insights, we propose a spike-based encoding algorithm that exploits neuronal variability to minimize network complexity and eliminates the need for external time references. Our method encodes continuous-time signals into spatio-temporal spiking patterns, with at most one spike per neuron (Fig. 1), using the DYNAP-SE mixed-signal neuromorphic hardware [26]. In this device, neurons are built using transistors in the linear domain, allowing low power con-

assumption. However, this is also introducing neuronal variability, referred to as 'device mismatch' [27]. Although mismatch is usually thought as a source of error and inaccuracy, in our encoding scheme, the mismatch itself is providing the required variability. Through simulations and hardware experiments, we evaluated the robustness and generalizability of the proposed encoding scheme. We observed the emergence of stereotyped sequences, coherently with what is observed in the cortex [9], and demonstrated successful decoding of multi-signal types in simulated environments. These findings not only underscore the relevance of variability-driven encoding for neuromorphic systems but also lay the foundation for its application in domains for which real-time processing is needed.

Results

The algorithm. Each continuous-time stimulus input to the network $x \in \mathcal{X}$ can be defined by both a time-series representation $x(t)$ and a parameter representation $x(p)$, with $p = (p_k)_{k=1\dots K}$. The proposed algorithm used a shallow network of exponential LIF (exp-LIF) neurons trained to encode stimulus parameters p when presented with the time series representation $x(t)$ (Fig.1). When stimulus $x(t)$ was sent to the shallow network, the first spike-time t_i of each neuron i was recorded, the population response $y = [t_1 \dots t_N]$ was re-referenced to the median \bar{t} and the encoded pattern $y^* = [t_1^* \dots t_N^*]$ with $t_i^* = t_i - \bar{t}$ was obtained. If a neuron did not fire after stimulus injection, its value was set to 0 after the re-referencing. The network was therefore encoding $x(t)$ with a temporal population coding $y^* \in \mathcal{Y}$. A linear decoder D was then trained to regress y^* to the stimulus parameter representation $x(p)$. During training (see Methods 7),

the decoding performance was computed as the Kendall-tau correlation between $x(p)$ and the decoded representation $\hat{x}(p)$. Such algorithm was implemented on both the DYNAP-SE neuromorphic hardware and on simulated networks, under three main conditions:

- Before injecting the stimulus into the network, the continuous signal was converted into a 2-dimensional spike stream with an Asynchronous Delta Modulator (ADM, see Methods 4 for details).
- Weights were defined as the number of connections between each pre-synaptic neuron to each postsynaptic one.
- Each neuron was characterized by an intrinsic time constant variability. Therefore, each neuron i had its own time constant value defined as $\tau_i = \tau + \eta_i^\tau * \tau$. On simulated networks η_i^τ was drawn from $\mathcal{N}(0, \sigma)$ with $\sigma = 0.2$. On DYNAP-SE the variability was provided by device mismatch, and it was shown to be comparable to the one implemented in simulations [27]. τ was shared between neurons.

The proposed encoding algorithm was implemented by a shallow network of N neurons with weight and time constants variability. To decode stimulus parameters, each network could optimize 3 time constants values (membrane time constant τ_{mem} , excitatory synapses τ_{syn_+} and inhibitory synapses τ_{syn_-} time constants) and $4N$ integer weights, for a total of $3 + 4N$ parameters.

As described in Methods 7, the network optimization proceeded iteratively, using a simple evolutionary algorithm. Time constants were randomly sampled from a spherical sampling volume [28]. The decoding score for each network configuration was computed and the best combination of time constant values was selected as the center of the sampling

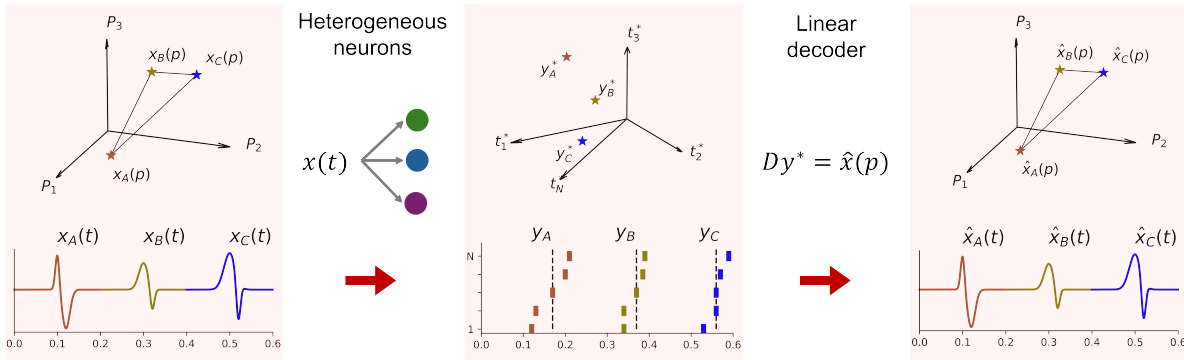


Figure 1. Continuous stimulus encoding with at most one spike per neuron. Stimuli $\{x\}$ were sampled from the stimulus parameter space and injected into a shallow network of N neurons. Each neuron was allowed to spike at most one spike upon receiving the stimulus. Each stimulus $(x_A(t), x_B(t), x_C(t))$ was encoded into an N -dimensional vector (y_A^*, y_B^*, y_C^*) with spike times of each neuron relative to the population median (dotted lines). The N -dimensional vector was then linearly regressed to the stimulus parameters.

volume for the next iteration of the algorithm. Network weights were progressively modified and tested. If the new network connectivity increased the score, the network was updated.

Stimulus encoding with analog neurons.

We implemented the proposed stimulus encoding on the DYNAP-SE neuromorphic chip [26] with 4 different synthetic signal types: “Gabor”, “Sinusoidal”, “SingleGauss” and “DoubleGauss”(as shown in Fig. 2A, see Methods 3). Synaptic weights and time constants were optimized to increase the performance of the linear decoder. Decoding performance was assessed with the Kendall-tau correlation between $x(p)$ and the decoded values $\hat{x}(p)$. Fig. 2 depicts the on-chip encoding algorithm performances for networks with 16 and 128 neurons, mediated over 3 different DYNAP-SE chips and 2 cores for each chip. As shown in Fig. 2B (blue dots), we obtained a mean 0.86 ± 0.04 Kendall-tau correlation on the best performing network size. We also decoded stimulus parameters using the first k principal components (PC) of the population response (red dots, principal component selection in Methods 6). For networks with 128 neurons, we

consistently achieved higher decoding accuracy with this decoding approach. We emphasize that PC projections were computed during training, and therefore the downstream decoding was still linear during testing. To assess the robustness of the method after network optimization and decoder training, we computed the Pearson correlation between $x(p)$ and $\hat{x}(p)$. We obtained high correlation on all datasets (mean Pearson $r = 0.93 \pm 0.02$) with small outlier percentage (mean % outliers = 1.0 ± 0.6 , see Methods 6 for outlier definition) as shown in Fig. 2C. Linear and non-linear stimulus parameters were linearly decoded from the proposed encoding scheme with high accuracy.

To justify the use of the first k PC for the stimulus decoding, we computed the Kendall-tau correlation as a function of the number of principal components (Fig. 2D). Adding principal components with high variance, the performance improved and then stabilized. However, adding low variance components, we noticed a decrease in the Kendall-tau correlation. Therefore, using the first k PC of the population response ensured a higher decoding accuracy.

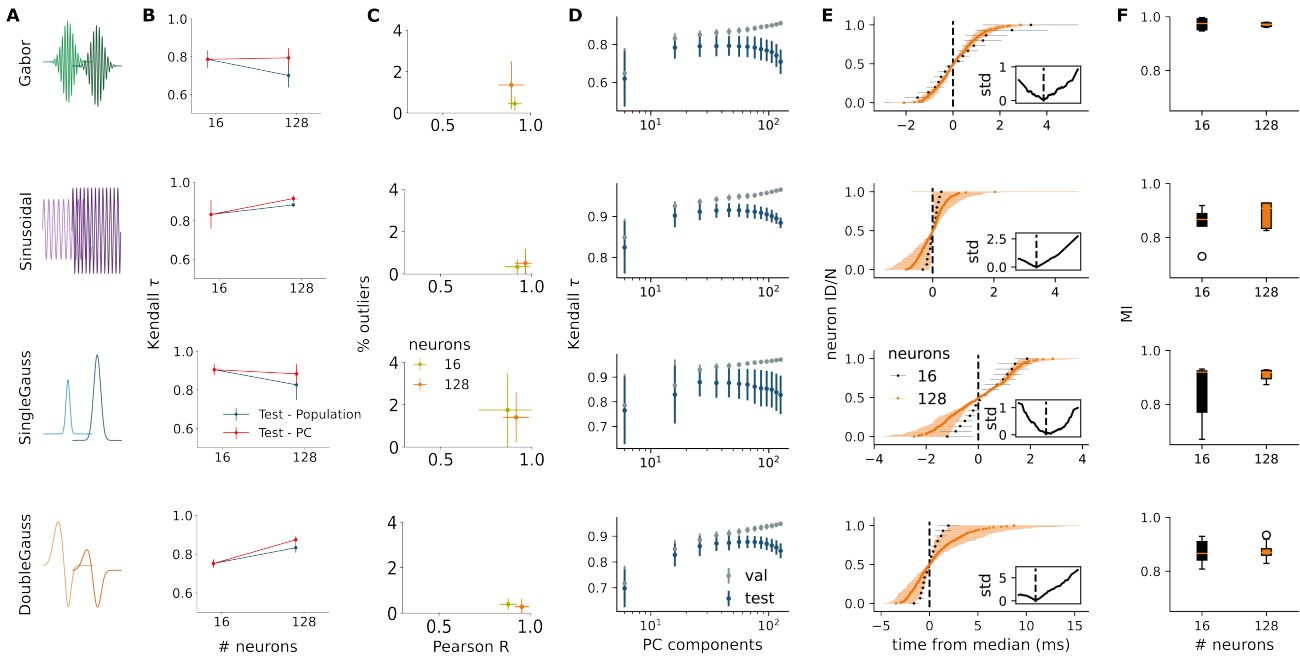


Figure 2. On-chip neural encoding performances across four synthetic signals. **A)** Example snippets for each synthetic signal type: Gabor, Sinusoidal, SingleGauss, and DoubleGauss. **B)** Kendall-tau correlation between the original and decoded stimulus parameters using the full population response (blue) or the first k principal components (PC, red) for two different neuron counts (16 and 128). **C)** Percentage of outliers and Pearson correlation for networks with 16 and 128 neurons. The decoding is performed using the first k PC of the population response. **D)** Kendall-tau correlation calculated in a transformed space via PCA, as a function of the number of principal components (experiment run on populations of 128 neurons). Adding low variance components, we observe a decrease in the Kendall-tau correlation. The overfit in A) for networks with 128 neurons originates from the decoder relying on low-variance principal components in the training set. **E)** Mean stereotyped spiking sequences for networks of 16 and 128 neurons for each input signal type. Inset: standard deviation between mean sequences with the same network size as a function of the distance from the median **F)** Mutation index (MI) for populations of 16 and 128 neurons, for each input signal type. A high MI value points to stereotyped spiking patterns.

On-chip stereotyped spiking sequences.

Within this framework, we investigated the spatio-temporal structure of the neural response to different stimuli. We computed the sorted mean activity for networks of 16 and 128 neurons for all signal types: coherently with what is recorded in the cortex [9], we observed the emergence of stereotyped sequences, characteristic for different input types (Fig. 2E). Furthermore, it was possible to observe a small variability between sequences in networks with the same size (Fig. 2E-inset), increasing with the time distance from the mean. We defined

the mutation index (MI) as the mean Kendall-tau correlation between sequences $\{y^*\}$ produced by trained networks. High MI values indicate the presence of stereotyped activity. For all signal types and network sizes we obtained an average $MI = 0.90 \pm 0.05$, (Fig. 2F). We could therefore conclude that the presented encoding scheme with analog neurons produced stereotyped spiking sequences.

On-chip encoding robustness. Neuronal variability is the core of the proposed algorithm. To quantitatively evaluate the robust-

ness to various amounts of variability and noise of such algorithm implemented on-chip, we proceeded as follows. First, to investigate how variability relates to encoding performance, we trained the linear decoder over the activity of progressively more homogeneous networks implemented on-chip, increasing the percentage of weight sharing between neurons (w^H). As expected, decreasing the network variability leads to worse encoding performances (Fig. 3A). Comparing networks with 16 and 128 neurons, it appears that both networks had similar behavior for the same absolute amount of variability. Considering relative variability reduction, larger networks were more robust. Furthermore, in Fig. 3B we evaluated the encoding robustness against random time jitters of the spiking activity, taking inspiration from the noisy communication within the brain. This has been tested by perturbing the spiking activity with gaussian noise sampled from $\mathcal{N}(0, \sigma)$ with increasing σ (from 0 to 1 ms). If noise was introduced already within the training set, test decoding was more robust to noisy activity than if noise was only included in test sets. Finally, we also tested the network robustness to noise introduced in the form of spike deletion (Fig 3C). In this test, the robustness increased with the network size.

Size and time constant analysis on simulated networks. In order to have full control on neuronal dynamics and variability, towards a complete understanding of the algorithm behavior and limitations, we have also evaluated such an algorithm within a simulated framework.

Specifically, we implemented simulations of networks of exp-LIF neurons with inhibitory and excitatory synapses with heterogeneous time constants and weights (see Methods 2). In a simulated environment we could monitor

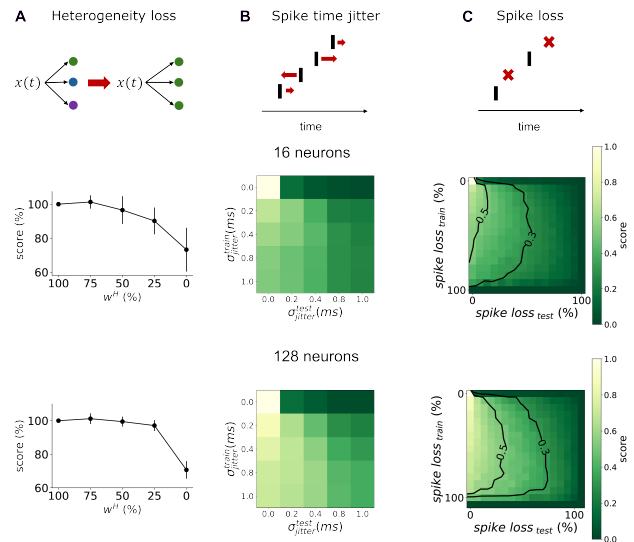


Figure 3. Impact of neuronal variability and noise on on-chip encoding performance. On-chip results assessing the algorithm robustness to variability reduction, temporal jitter and spike deletion on DoubleGauss signal decoding. **First row)** graphical representation of the robustness experiment. **Second row)** results from on-chip measurement for networks with 16 analog neurons. **Third row)** results from on-chip measurement for networks with 128 analog neurons. For all tests, the score was computed as the percentage of the Kendall-tau correlation in the unperturbed case. **A)** Kendall-tau correlation as a function of weight variability ($w^H(\%)$). **B)** Kendall-tau correlation heatmap illustrating the influence of a temporal jitter applied during the training and testing phases. **C)** Kendall-tau correlation score heatmap illustrating the influence of spike deletion applied during the training and testing phases.

time constant values for different signal types and network sizes. As shown in Fig. 4A, optimizing simulated networks with a wide array of network sizes, we observed an increase in Kendall-tau correlation with network size when decoding using the first k PC of the population response. Decoding with PC, we obtained a mean Kendall correlation 0.93 ± 0.03 on the best performing network size. Analogously, the Pearson correlation between $x(p)$ and $\hat{x}(p)$ increased with the network size (Fig. 4B). We obtained a mean Pearson

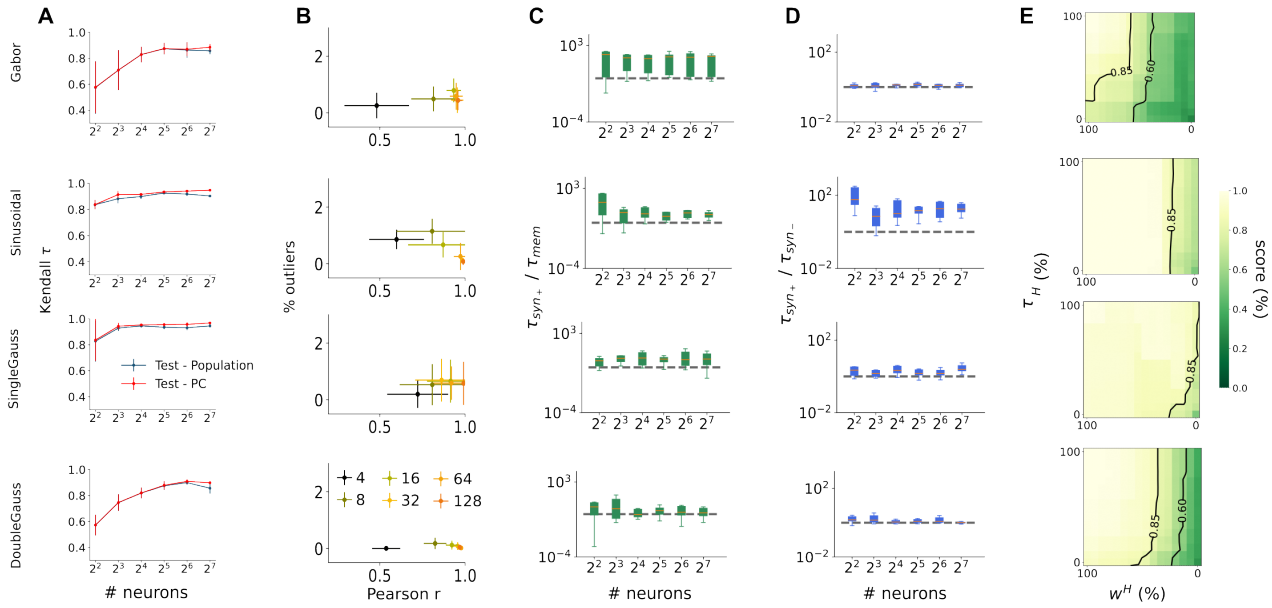


Figure 4. Encoding algorithm characterization on simulated networks. Single-spike encoding algorithm leveraging the variability of a simulated shallow network of exp-LIF neurons tested on the same input signal types used for on-chip testing (rows). **A)** Kendall-tau correlation between original and decoded stimulus for networks with an increasing number of neurons. Stimulus decoding with the first k principal components (PC) showed improved correlation increasing the network size. **B)** Percentage of outliers and Pearson correlation for all trained networks. The decoding is performed using the first k PC of the population response. **C, D)** Trained neuron parameters (ratio between time constant of excitatory synapses τ_{syn+} and membrane time constant τ_{mem} and ratio between excitatory τ_{syn+} and inhibitory τ_{syn-} time constants respectively) as a function of neuron population size. **E)** Kendall-tau correlation heat-map as a function of variability loss in the weights ($w^H(\%)$) and time constants ($\tau^H(\%)$). Weight variability had stronger impact on performance than time constant variability.

correlation $r = 0.92 \pm 0.03$ with $\%$ outliers $= 0.2 \pm 0.2$ on the best performing network size. We then evaluated the ratio between time constant values for different network sizes (Fig. 4C and D). These observables showed that, on average, for each signal type the optimization procedure converged to $\tau_{syn+} \geq \tau_{syn-} \geq \tau_{mem}$. Being able to control both weight and time constant variability, we expanded the variability robustness results shown in Fig. 3A and tested which kind of variability drives encoding performance the most (Fig. 4E). For all signal types, weights had a stronger effect on performance than time constants. However, optimizing both types of variability led to the highest encoding

performances. To test the presence of stable spiking patterns in simulated networks, we computed their cosine similarity for different network sizes for each signal type. Considering all signal types, we obtained a mean 0.8 ± 0.1 cosine similarity: spiking patterns were therefore stable for different network sizes.

Stereotyped spiking sequences are signal-type specific.

When presenting visual stimuli to humans, cortical spiking sequences appear to be stimulus-type specific [9]. We tested if networks trained on one stimulus type were able to produce different patterns for other types of stimuli. Injecting all 4 stimulus types into simulated trained networks, we ob-

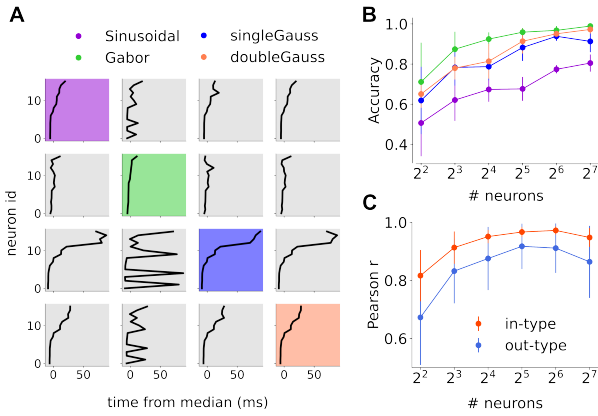


Figure 5. Stimulus-specific spiking patterns in one simulated network. **A)** We injected stimuli from all 4 signal types into one simulated trained network and obtained the mean spiking order for each stimulus type. Each row represents the mean spiking activity for stimulus type i , sorted according to the mean spiking order of stimulus type j . **B)** Linear decoding of stimulus type from the encoding of one network. **C)** Linear decoding of stimulus parameters for all stimulus types in one network. Pearson r was higher for the stimulus type the network has been trained on (in-type) compared to the mean of the other stimulus types (out-type). On average, Pearson r increased with the network size till a plateau was reached.

served the presence of 4 different stereotyped sequences. (Fig. 5A).

We then tested if stimulus type could be linearly decoded at the single trial level from the proposed encoding. On average, we observed an increase in the decoding accuracy when increasing the network size (Fig. 5B).

We then assessed the linear decoding accuracy of stimulus parameters for all stimulus types in one network (Fig. 5C). For all networks, the Pearson correlation was higher for the stimulus type the network has been trained on (in-type) compared to all the other types (out-type). On average, increasing the network size we achieved higher decoding accuracy (Fig.4).

Discussion

This work introduced an algorithm for continuous-time signal encoding that leverages the variability of exp-LIF neuron populations to produce robust spatio-temporal patterns with at most one spike per neuron. Building on the principles of neuronal variability and spike-based encoding [23, 13], our approach minimizes network complexity by exploiting the intrinsic variability of the analog neuromorphic hardware. By aligning with the observed features of some cortical circuits [7, 8, 9], where stimulus information is encoded into precise spatio-temporal spiking patterns, this method bridges theoretical neuroscience and practical neuromorphic implementations.

The proposed method demonstrates robust performance, supporting the linear decoding of multiple parameters, both linear and nonlinear. The compatibility with the DYNAP-SE mixed-signal neuromorphic platform highlights its adaptability to challenging neuromorphic hardware. Furthermore, the insights gained from synthetic simulations extend to hybrid analog-digital systems and emerging unconventional computing frameworks. Future work will explore the application of this algorithm to other spiking processors, which may provide additional flexibility and scalability.

The algorithm employs the median spike time as an internal clock, avoiding dependence on external time references or stimulus onset markers [22, 21]. This population-driven timing aligns with biological evidence of reliable temporal coding through population activity [29] and gives always-on capabilities to the encoder. The compact, spike-based representations and the linear downstream decoding not only minimize computational overhead but also enable fast information

retrieval.

While this study validates the algorithm through synthetic simulations and implementation on DYNAP-SE hardware, it has not been extensively tested with real-world data. Future research will focus on applying the method to practical scenarios as biomedical signal processing. Another limitation is the current single-spike-per-neuron constraint, which, while computationally efficient, may limit the richness of encoded representations. Future research may examine the impact of relaxing this constraint to allow for more flexible encoding schemes, tailored to specific tasks.

In summary, this study presents a robust, brain-inspired method for encoding continuous stimuli into compact spike-based representations. By leveraging neuronal variability and precise spike timing, this low-complexity approach offers low-latency, always-on capabilities for neuromorphic signal processing and bridges the gap between biological principles, computational models, and technological applications.

Methods

1. DYNAP-SE

DYNAP-SE is a multi-core asynchronous mixed signal neuromorphic processor. Each of the 4 cores comprises 256 adaptive exponential Leaky Integrate & Fire (LIF) silicon neurons with two excitatory and two inhibitory analog synapses. In the limit of high input current and shutting off the adaptation, the neural dynamics of the DYNAP-SE LIF can be expressed as:

$$\tau \frac{d}{dt} I_{\text{mem}} + I_{\text{mem}} \approx \frac{I_{\text{in}} I_{\text{gain}}}{I_{\tau}} + \frac{I_a I_{\text{mem}}}{I_{\tau}}$$

where I_{mem} is the membrane potential,

τ is the neuron time constant, and $\frac{I_a I_{\text{mem}}}{I_{\tau}}$ models the positive feedback block. Each neuron has a 64 connections fan-in and 1024 connections fan-out. Neurons in each DYNAP-SE core share bias settings and, therefore, time constant values are shared.

2. Neuron model on simulated network

We used the exponential leaky integrate-and-fire (exp-LIF) neuron model for the simulated networks. The neuron has a membrane time constant defined as τ_{mem} , firing when the membrane potential $V(t)$ reaches the threshold θ . The neuron dynamics is defined as:

$$\begin{aligned} \frac{dV(t)}{dt} &= -\frac{V(t)}{\tau_{\text{mem}}} + I_{\text{syn}}(t) \\ I_{\text{syn}}(t) &= -I_{-}(t) + I_{+}(t) \\ \frac{dI_{+}(t)}{dt} &= -\frac{I_{+}(t)}{\tau_{\text{syn}+}} + w_{+}^{UP} \sum_i \delta(t - t_i^{UP}) + \\ &\quad + w_{+}^{DN} \sum_i \delta(t - t_i^{DN}) \\ \frac{dI_{-}(t)}{dt} &= -\frac{I_{-}(t)}{\tau_{\text{syn}-}} + w_{-}^{UP} \sum_i \delta(t - t_i^{UP}) + \\ &\quad + w_{-}^{DN} \sum_i \delta(t - t_i^{DN}) \end{aligned}$$

Each neuron i can fire at most one spike when its voltage threshold is reached. To address chip compatibility, synaptic weights w can assume only integer values. The neurons have heterogeneous properties. In a population of N neurons, only one value can be assigned for each time constant ($\tau_{\text{mem}}, \tau_{\text{syn}+}, \tau_{\text{syn}-}$). Each simulated neuron i has an intrinsic variability given by a multiplicative noise term. For a given neural time constant τ , neuron i presents the following parameter value: $\tau_i = \tau + \eta_i^{\tau} * \tau$

where $\eta_i^{\tau} \sim \mathcal{N}(0, \sigma)$ with $\sigma = 0.2$. The results presented an average across 10 different

neural population instances.

All simulated neurons are provided with two kinds of synapses: one excitatory with synaptic time constant $\tau_{\text{syn}+}$ and one inhibitory with synaptic time constant $\tau_{\text{syn}-}$. On DYNAP-SE, when a large input current is provided, neurons follow the same dynamics as in the simulation [30] but with a current-based positive feedback that drives spike generation.

The simulation framework we developed allows for customizable neuron models, network configurations, and variability conditions, making it applicable to a broad range of neuromorphic systems. By simulating different levels of heterogeneity and noise, it provides a robust testing environment for evaluating encoding algorithms beyond the DYNAP-SE hardware.

3. Datasets

On DYNAP-SE and on simulated networks, we considered 4 signal types:

- Sinusoidal stimulus:

$$x(t) = p_1 \sin(2\pi p_2 t)$$

with $p_1 \in [5, 10)$, $p_2 \in [500, 1500)$ Hz on DYNAP-SE and $p_1 \in [1, 6)$, $p_2 \in [10, 100)$ Hz on simulation.

- Gabor stimulus:

$$x(t) = 3e^{-\frac{t^2}{2p_1^2}} \sin(2\pi p_2 t)$$

with $p_1 \in [2, 3)$ ms, $p_2 \in [500, 1500)$ Hz on DYNAP-SE and $p_1 \in [20, 40)$ ms, $p_2 \in [10, 100)$ Hz on simulation.

- SingleGauss stimulus:

$$x(t) = p_1 e^{-\frac{t^2}{2p_2^2}}$$

with $p_1 \in [1, 6)$, $p_2 \in [0.2, 1.3)$ ms on DYNAP-SE and $p_1 \in [1, 6)$, $p_2 \in [10, 30)$ ms on simulation.

- DoubleGauss stimulus:

$$x(t) = p_1 e^{-\frac{t^2}{2p_2^2}} + p_3 e^{-\frac{(t-0.02)^2}{2p_4^2}}$$

with $p_1, p_3 \in [1, 3)$, $p_2, p_4 \in [0.6, 1)$ ms on DYNAP-SE and $p_1, p_3 \in [1, 3)$, $p_2, p_4 \in [4, 10)$ ms on simulation.

On DYNAP-SE, each stimulus injection lasts for 10 ms with a sampling frequency $f_s = 5e4$. On simulation, each stimulus injection lasts for 200 ms with a sampling frequency $f_s = 5e3$.

Sampling frequency on DYNAP-SE is chosen to allow fast processing. Parameters are chosen to guarantee optimal ADM conversion with the predefined sampling frequency.

Error bars in Fig.2 are computed as one standard deviation for 6 different hardware networks. Error bars in Fig.4 are computed as one standard deviation for 10 different simulated networks.

4. ADM converter

Stimuli are converted into spikes using an asynchronous delta modulator (ADM) before injection into a population of neurons. For each stimulus $x(t)$, we consider its reference value $x(0)$ and two thresholds at $x(0) + \delta$ (UP threshold) and $x(0) - \delta$ (DN threshold). If the signal at time t^* crosses the UP (DN) threshold, a UP (DN) event is generated at time t^* , and the UP/DN thresholds are updated as $x(t^*) + \delta$ and $x(t^*) - \delta$. This process converts each stimulus into a stream of UP and DN events. We can then obtain the ADM-reconstructed version of the stimulus $\tilde{x}(t)$ from the stream of UP/DN events. From $\tilde{x}(0) = 0$, we update the stimulus amplitude every time a UP/DN event occurs. If a UP event occurs at time t^* , then $\tilde{x}(t^*) = \tilde{x}(t^* - 1) + \delta$ ($-\delta$ for a DN event). The optimal ADM threshold value is determined by

maximizing the Pearson correlation between Euclidean distances of stimuli computed from the continuous dataset and their reconstructed version.

5. Encoding algorithm

Stimulus $x(t)$ has a parameter representation $x(p) = (p_1 \dots p_K)$. When the ADM-converted stimulus $x(t)$ is injected into a population of N neurons, a spiking output $y(t)$ is produced, where y_i is equal to the firing time of neuron i . If neuron j does not fire, then $y_j = 0$. Firing times are then re-referenced to the median m of active neurons' firing times. Therefore, each stimulus $x(t)$ is mapped to an N -dimensional vector y^* defined as:

$$\begin{cases} y_i^* = y_i - m & \text{if } y_i \neq 0 \\ y_i^* = 0 & \text{if } y_i = 0 \end{cases}$$

6. Linear decoding

A linear regression is performed from the encoded signal y^* to the stimulus parameters $x(p) = (p_1 \dots p_K)$. To assess the performance of the linear decoder, we compute the Kendall-tau correlation between stimulus parameters $x(p) = (p_1 \dots p_K)$ and decoded parameters $\hat{x}(p) = (\hat{p}_1 \dots \hat{p}_K)$. We also compute the Pearson correlation between $x(p)$ and $\hat{x}(p)$ after removing outliers, defined as $\hat{x}(p)$ values bigger than twice the largest $x(p)$, or smaller than half the smallest $x(p)$. When decoding using principal components, we performed the following steps: we first performed PCA on the population response of the training set; we then assessed the decoding accuracy on a validation set, progressively increasing the number of principal components. The first k principal components for which we obtained the highest validation accuracy were then used for testing. Since we performed

PCA only during training, and we kept the linear projection fixed during testing, the final downstream decoding is still linear.

7. Optimization protocol

Network optimization follows two main steps:

- Neural time constants $\{\tau_{mem}, \tau_{syn+}, \tau_{syn-}\}$ are sampled from a uniform distribution with radius r . The Kendall-tau correlation of each network configuration is evaluated, and the best-performing set of time constants is set as the center of the new sampling space.
- Weights are integer values that can be changed as follows: First, a neuron index i is randomly extracted. This neuron can then change its excitatory and/or inhibitory weights by an amount that goes from ± 1 to ± 4 .

The score of each parameter set is defined as the Kendall-tau correlation between input and decoded parameters.

8. Stereotyped spiking sequences

For each signal type and network size, we compute the mean spiking sequence over all stimuli. The neurons are then re-ordered based on their mean spike time in ascending order. The consistency of the spiking sequences is assessed with the mutation index (MI), defined as the mean Kendall-tau correlation between the mean spiking sequence and the single trial sequences. To test the independence of the spiking pattern on the network size, we first computed the spiking sequences for all network sizes and repetitions. We then created, for each network size, one histogram with the spike times of all sequences. After scaling, we removed the mean from each histogram

and computed the cosine similarity between histograms.

9. Robustness

The robustness of the encoding is tested by making the trained network progressively more homogeneous. Time constants homogeneity is increased by randomly selecting one neuron in the population and setting its time constant values as the mean of the time constants of the population. Weight homogeneity follows the same reasoning, setting the weight of randomly selected neurons as the mean of the weights of the population.

The robustness of the encoding is also tested against random temporal jitters in the spike times. After recording all spike times for all stimuli, we applied temporal jitters sampled from $\mathcal{N}(0, \sigma)$ with $\sigma = [0.2, 0.4, 0.8, 1]$ ms to the training and/or test set. We then trained the linear decoder and assessed the performance with the Kendall-tau correlation.

Robustness to spike deletion is assessed by removing spikes from randomly selected neurons for each stimulus encoding. After spike removal, the activity of the population is re-referenced to the new median of active neurons' spike times and a linear decoder is trained and tested on the perturbed spiking sequences.

Results presented in Fig.3 are obtained from experiments with DoubleGauss signals and 4 different hardware networks.

Acknowledgments

Part of this work has been done within the 2024 CapoCaccia Neuromorphic Workshow. C.D.L has received funding from Bridge Fellowship founded by the Digital Society Initiative at University of Zurich (grant

no.G-95017-01-12); F.C. was funded by the Swiss National Science Foundation (grant no. 204651) and received UZH Candoc Grant (grant no. FK-24-025). We thank Prof. Dr. Giacomo Indiveri and Prof. Dr. Johannes Sarnthein for the valuable guidance, support and useful discussions.

References

- [1] John J Hopfield. Pattern recognition computation using action potential timing for stimulus representation. *Nature*, 376(6535):33–36, 1995.
- [2] Edmund Chong, Monica Moroni, Christopher Wilson, Shy Shoham, Stefano Panzeri, and Dmitry Rinberg. Manipulating synthetic optogenetic odors reveals the coding logic of olfactory perception. *Science*, 368(6497):eaba2357, 2020.
- [3] Mircea I Chelaru and Valentin Dragoi. Efficient coding in heterogeneous neuronal populations. *Proceedings of the National Academy of Sciences*, 105(42):16344–16349, 2008.
- [4] Karim G Habashy, Benjamin D Evans, Dan FM Goodman, and Jeffrey S Bowers. Adapting to time: why nature evolved a diverse set of neurons. *arXiv preprint arXiv:2404.14325*, 2024.
- [5] Zachary F Mainen and Terrence J Sejnowski. Reliability of spike timing in neocortical neurons. *Science*, 268(5216):1503–1506, 1995.
- [6] Artur Luczak, Peter Bartho, and Kenneth D Harris. Gating of sensory input by spontaneous cortical activity. *Journal of Neuroscience*, 33(4):1684–1695, 2013.
- [7] Artur Luczak, Bruce L McNaughton, and Kenneth D Harris. Packet-based communication in the cortex. *Nature Reviews Neuroscience*, 16(12):745–755, 2015.
- [8] Alex P Vaz, John H Wittig Jr, Sara K Inati, and Kareem A Zaghloul. Backbone spiking sequence as a basis for preplay, replay, and default states in human cortex. *Nature Communications*, 14(1):4723, 2023.
- [9] Weizhen Xie, John H Wittig Jr, Julio I Chapeton, Mostafa El-Kalliny, Samantha N Jackson, Sara K Inati, and Kareem A Zaghloul. Neuronal sequences in population bursts encode information in human cortex. *Nature*, pages 1–8, 2024.
- [10] Nicolas Perez-Nieves, Vincent CH Leung, Pier Luigi Dragotti, and Dan FM Goodman. Neural heterogeneity promotes robust learning. *Nature communications*, 12(1):5791, 2021.
- [11] Xueyuan She, Saurabh Dash, and Saibal Mukhopadhyay. Sequence approximation using feedforward spiking neural network for spatiotemporal learning: Theory and optimization methods. In *International Conference on Learning Representations*, 2021.
- [12] Richard Gast, Sara A Solla, and Ann Kennedy. Neural heterogeneity controls computations in spiking neural networks. *Proceedings of the National Academy of Sciences*, 121(3):e2311885121, 2024.
- [13] Fleur Zeldenrust, Boris Gutkin, and Sophie Denève. Efficient and robust coding in heterogeneous recurrent networks. *PLoS computational biology*, 17(4):e1008673, 2021.
- [14] Sebastian Gerwinn, Jakob H Macke, and Matthias Bethge. Bayesian population decoding of spiking neurons. *Frontiers in computational neuroscience*, 3:648, 2009.
- [15] Aurel A Lazar. Time encoding with an integrate-and-fire neuron with a refractory period. *Neurocomputing*, 58:53–58, 2004.
- [16] Aurel A Lazar and Eftychios A Pnevmatikakis. Reconstruction of sensory stimuli encoded with integrate-and-fire neurons with random thresholds. *EURASIP Journal on Advances in Signal Processing*, 2009:1–14, 2009.
- [17] Karen Adam, Adam Scholefield, and Martin Vetterli. Sampling and reconstruction of bandlimited signals with multi-channel time encoding. *IEEE Transactions on Signal Processing*, 68:1105–1119, 2020.
- [18] Benjamin Schrauwen and Jan Van Campenhout. Bsa, a fast and accurate spike train encoding scheme. In *Proceedings of the International Joint Conference on Neural Networks, 2003.*, volume 4, pages 2825–2830. IEEE, 2003.
- [19] M Rabinovich, A Volkovskii, P Lecanda, R Huerta, HDI Abarbanel, and G Laurent. Dynamical encoding by networks of competing neuron groups: winnerless competition. *Physical review letters*, 87(6):068102, 2001.
- [20] Dean V Buonomano and Michael M Merzenich. Temporal information transformed into a spatial code by a neural network with realistic properties. *Science*, 267(5200):1028–1030, 1995.
- [21] Ana Stanojevic, Stanisław Woźniak, Guillaume Bellec, Giovanni Cherubini, Angeliki Pantazi, and Wulfram Gerstner. High-performance deep spiking neural networks with 0.3 spikes per neuron. *Nature Communications*, 15(1):6793, 2024.
- [22] Julian Göltz, Laura Kriener, Andreas Baumbach, Sebastian Billaudelle, Oliver Breitwieser, Benjamin Cramer, Dominik Dold, Akos Fer-

- enc Kungl, Walter Senn, Johannes Schemmel, et al. Fast and energy-efficient neuromorphic deep learning with first-spike times. *Nature machine intelligence*, 3(9):823–835, 2021.
- [23] Sophie Denève and Christian K Machens. Efficient codes and balanced networks. *Nature neuroscience*, 19(3):375–382, 2016.
- [24] Martin Boerlin, Christian K Machens, and Sophie Denève. Predictive coding of dynamical variables in balanced spiking networks. *PLoS computational biology*, 9(11):e1003258, 2013.
- [25] E Paxon Frady and Friedrich T Sommer. Robust computation with rhythmic spike patterns. *Proceedings of the National Academy of Sciences*, 116(36):18050–18059, 2019.
- [26] Saber Moradi, Ning Qiao, Fabio Stefanini, and Giacomo Indiveri. A scalable multicore architecture with heterogeneous memory structures for dynamic neuromorphic asynchronous processors (dynaps). *IEEE transactions on biomedical circuits and systems*, 12(1):106–122, 2017.
- [27] Dmitrii Zendrikov, Sergio Solinas, and Giacomo Indiveri. Brain-inspired methods for achieving robust computation in heterogeneous mixed-signal neuromorphic processing systems. *Neuromorphic Computing and Engineering*, 3(3):034002, 2023.
- [28] Filippo Costa, Eline V Schaft, Geertjan Huiskamp, Erik J Aarnoutse, Maryse A van’t Klooster, Niklaus Krayenbühl, Georgia Ramantani, Maeike Zijlmans, Giacomo Indiveri, and Johannes Sarnthein. Robust compression and detection of epileptiform patterns in ecog using a real-time spiking neural network hardware framework. *Nature Communications*, 15(1):3255, 2024.
- [29] Steven M Chase and Eric D Young. First-spike latency information in single neurons increases when referenced to population onset. *Proceedings of the National Academy of Sciences*, 104(12):5175–5180, 2007.
- [30] Elisabetta Chicca, Fabio Stefanini, Chiara Bartolozzi, and Giacomo Indiveri. Neuromorphic electronic circuits for building autonomous cognitive systems. *Proceedings of the IEEE*, 102(9):1367–1388, 2014.